Model Predictive Path-Following Control for Airborne Wind Energy Systems ⋆

Sanket Diwale * **Timm Faulwasser** ** **Colin N. Jones** *

* *Laboratoire d'Automatique, École Polytechnique Fédérale de Lausanne, Switzerland. e-mail: {sanket.diwale, colin.jones}@epfl.ch*
** *Institute for Applied Computer Science, Karlsruhe Institute of Technology, Karlsruhe, Germany. e-mail: timm.faulwasser@kit.edu*

Abstract: A nonlinear path following model predictive control scheme with application to a kite based airborne wind energy system is presented. A novel terminal constraint is introduced to guarantee closed-loop stability and convergence of the vehicle to geometric paths of desired shapes. Convergence conditions are investigated and the efficacy of the approach is demonstrated via numerical simulations for desired path shapes under nominal and perturbed conditions.

Keywords: nonlinear model predictive control, path following, convergence vector field

1. INTRODUCTION

A common operational requirement for kite based Airborne Wind Energy (AWE) systems is to track a desired optimal trajectory that maximizes power generation. This requires the kite to reel out at a desired rate as it flies a high energy extraction trajectory, then reel back in with a low energy consumption maneuver such that a net positive energy generation cycle is exhibited (Luchsinger, 2013; Loyd, 1980).

While the desired trajectory for the vehicle can be precomputed using numerical optimal control solvers (Houska and Diehl (2007, 2010); Erhard et al. (2015)), the trajectory tracking itself presents numerous challenges due to nonholonomic properties of the system, uncertain wind and system parameters and limited controllability of the vehicle speed. In fact, since the main driving force is provided by the wind, the vehicle can only follow time-profiles along the reference path that are coherent with the wind. Previous works, like Ilzhfer et al. (2007); Gros et al. (2013) consider Nonlinear Model Predictive Control (NMPC) schemes tracking reference positions given as a time parameterized reference trajectory. The effects of unknown wind conditions, however, limit the applicability of such schemes as the reference trajectory can quickly become inconsistent with the wind speed and kite position, leading to non zero tracking errors. Erhard and Strauch (2014); Fagiano et al. (2014) overcome this issue of incoherence by changing the reference only on certain position feedback switching events. They do not, however, consider any exact reference trajectory or path shape to be followed. Diwale et al. (2016) tackles this issue by considering a path-following scheme based on feedback linearization of the AWE system. The feedback linearization scheme however provides only a localized region of attraction in the presence of input saturation and leads to suboptimal control demands due to cancellation of all natural dynamics of the vehicle.

Motivated by these observations, we propose a Model Predictive Path-Following Control (MPFC) scheme inspired by Faulwasser and Findeisen (2016) to plan for feasible trajectories guaranteeing convergence and tracking of the reference path. The core idea of MPFC is to consider a geometric reference path instead of a time-parametrized reference trajectory. A virtual system is used to control the motion of a reference point along the path. Finally, the input to the virtual system and the real system input are computed by means of receding horizon optimization such that the path is followed as closely as possible. In order to guarantee path convergence, we consider terminal constraints, which are inspired by vector field control schemes often used in aerial vehicles or mobile robots (Panagou et al., 2011). The advantage of incorporating such constraints in the MPC scheme is that we do not need an explicit representation of the vector field.

The organization of the paper is as follows. Section 2 defines the problem statement. Section 3 discusses the design of the proposed MPFC scheme. Section 4 provides the proof sketch for stability and recursive feasibility of the MPFC scheme subject to a reachability assumption for the convergence field. Section 5 presents simulation results under nominal and perturbed conditions.

Notation

$\|v\|$	2-norm of a vector($\|v\| := \sqrt{v^T v}$)
$\|v\|_Q$	Weighted 2-norm($\|v\|_Q := \sqrt{v^T Q v}, Q > 0$)
$\text{atan2}(\cdot,\cdot)$	Four quadrant inverse tangent
$\partial_\tau f$	Partial derivative of a function f w.r.t. τ

2. PROBLEM STATEMENT

Recall that the core idea of MPFC is to coordinate the control of the real vehicle and the reference speed along a path such that the tracking error is minimized. In order to

⋆ This work is funded by the Sinergia project "Autonomous Airborne Wind Energy" (A^{2}WE) of the Swiss National Science Foundation (SNSF).

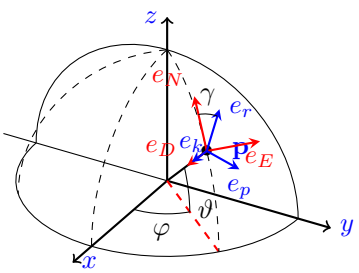

Fig. 1. Kite coordinate frames representation.

precisely define this objective for path following in AWE systems, we describe the model of the AWE system and the virtual system used to control the reference motion along the path. We then define the path-following problem.

2.1 Kite Model

The vehicle for the AWE system moves on a sphere of radius L (tether length). Its position in polar coordinates is given by the elevation and azimuth angles ϑ, φ. We denote by γ the direction of the tangential velocity of the vehicle on the sphere. By simple geometric relations, the angle γ can be written as,

$$\gamma = \text{atan2}(\dot{\varphi}\cos\vartheta, \dot{\vartheta}) \tag{1}$$

Denoting the state of the vehicle at time t as $q(t) := (\vartheta(t), \varphi(t), \gamma(t))$, we can write the vehicle dynamics as,

$$\dot{q} = s(q, \lambda, L, z)\begin{pmatrix}\cos\gamma\\ \sin\gamma\\ 0\end{pmatrix} + \begin{pmatrix}0\\0\\u_\gamma\end{pmatrix} \tag{2}$$

where $s(q, p, L, z) : \mathcal{Q} \times \Lambda \times \mathbb{R} \times \mathbb{R} \to \mathbb{R}^+$ is the physical speed of the kite as a function of the vehicle state $q \in \mathcal{Q}$, physical parameters $p \in \Lambda$ comprising the wind speed and aerodynamic parameters, tether length L and the reel out rate $\dot{L} = z$. u_γ is a steering input to the system that allows us to turn the vehicle ($\dot{\gamma} = u_\gamma$). We refer the reader to Figure 1 for a graphical representation of the angles and to Diwale et al. (2016) for details on this model. The specifics of $s, \mathcal{Q}, \Lambda$ are given in the Appendix.

Remark 1. For simplicity of exposition, we assume that the tether length L is fixed and the reel out rate $z = 0$. We treat any deviation from this assumption as a perturbation. □

2.2 Reference Path

For the reference path we consider any twice continuously differentiable *periodic* mapping $q_{ref}(\tau) : \mathbb{R} \to \mathcal{Q}$ satisfying the assumptions below.

Assumption 1. (Nonholonomic constraint). The reference path is such that $\gamma_{ref} = \text{atan2}(\partial_\tau\varphi_{ref}\cos\vartheta_{ref}, \partial_\tau\vartheta_{ref})$. □

Thus the reference path γ_{ref} satisfies the same geometric relation with $\vartheta_{ref}, \varphi_{ref}$ as (1). This assumption is satisfied by any path for which we choose $\vartheta_{ref}(\tau), \varphi_{ref}(\tau)$ and then compute $\gamma_{ref}(\tau)$ as given above.

Assumption 2. (Regular curve). The path is regular in the sense that for all τ we have $||\partial_\tau q_{ref}(\tau)|| \neq 0$. □

Thus the reference $q_{ref}(\tau)$ does not remain stationary as τ changes. In other words, locally each point on the path corresponds to a unique τ, cf. Topogonov (2006).

Assumption 3. (Compact range). The path parametrization $q_{ref} : \mathbb{R} \to \mathcal{Q}$ has a compact range in $\mathcal{Q}$. □

Thus $q_{ref}(\tau)$ attains a value for each τ within $\mathcal{Q}$, avoiding unbounded reference trajectories and limiting behavior where the limiting value does not lie in $\mathcal{Q}$.

Assumption 4. (Input admissibility). The reference path curvature is limited such that it can be tracked at a given vehicle speed while respecting the steering constraints. □

Assumption 4 allows only those reference paths which can be tracked by the real vehicle at a given speed s with limited steering input u_γ^{max} when starting with zero tracking error. Due to space limitations, we skip the details of verifying this assumption.

We move a virtual point along the path by moving τ with controlled velocity u_τ with the dynamics,

$$\dot{\tau} = u_\tau \tag{3}$$

We enforce $u_\tau \geq 0$ to make the virtual vehicle move in a fixed direction along the path.

2.3 Kite Path-Following Problem

We consider the augmented system of the virtual point and real vehicle with the state

$$x(t) := (q(t), \tau(t)).$$

The dynamics of $x(t)$ is then given by (2), (3). We define the path error for q and $q_{ref}(\tau)$ for an arbitrary q, τ as

$$e(q, \tau) = q - q_{ref}(\tau). \tag{4}$$

For $q(t), \tau(t)$, we denote path-following error at time t as

$$e(t) = q(t) - q_{ref}(\tau(t)). \tag{5}$$

For notational convenience, we denote the tangent to the reference path as $m(\tau) = \partial_\tau q_{ref}(\tau)$. The control objective is then to asymptotically drive $e(t)$ to 0 as $t \to \infty$ subject to the constraints (2–3) and the actuator constraint set

$$\mathcal{U} = \{(u_\tau, u_\gamma)^T \in \mathbb{R}^2 \,|\, u_\tau \geq 0, \quad |u_\gamma| \leq u_\gamma^{max}\}.$$

3. MODEL PREDICTIVE PATH FOLLOWING CONTROL

As standard in NMPC, MPFC is based on receding horizon solutions to an Optimal Control Problem (OCP). Here, we consider MPFC based on the following OCP:

$$\min_{x(\cdot),u(\cdot)} \quad \int_0^T \frac{1}{2}||e(s)||_Q^2 + ||u(s)||_R^2 ds + \frac{1}{2}||e(T)||_{Q_f}^2 \tag{6a}$$

$$\text{subject to } (2), (3) \quad \text{with } x(0) = \hat{x}(t) \tag{6b}$$

$$u(s) \in \mathcal{U}, x(s) \in \mathcal{X} \quad \forall s \in [0, T] \tag{6c}$$

$$\frac{1}{2}||e(T)||_Q^2 + e(T)^T Q_f \dot{q}(T) \leq 0. \tag{6d}$$

$$e(q(T), \tau(T))Q_f m(\tau(T)) \geq 0 \tag{6e}$$

where $\mathcal{X} := \mathcal{Q} \times \mathbb{R}$, and $\hat{x}(t)$ denotes the systems state at time t under the closed-loop control action of the MPFC scheme. The OCP is solved in receding horizon

fashion at time t.[1] The actual input applied to the system $\hat{u}(t)$ is given by $\hat{u}(t) = u^\star(0)$ for the optimal solution $u^\star(\cdot)$ of the OCP at time t. As will be shown later, the constraints (6e),(6d) correspond to the existence of a vector field controller and is used to provide a larger region of attraction to the MPFC scheme. The matrices Q, Q_f are chosen to be symmetric positive definite.

The next result certifies the path convergence properties of the MPFC scheme based on OCP (6).

Proposition 1. (Path convergence). Consider the MPFC scheme based on (6). Let the prediction model (2) be an exact representation of the kite dynamics, i.e. there is no plant-model mismatch. Suppose that OCP (6) is feasible for all $t \geq 0$. Then, the closed loop satisfies

$$\lim_{t\to\infty} \|e(t)\| = 0. \qquad \square$$

Proof. Due to space limitations, we sketch only the main steps of the proof. Consider the positive semi-definite value function $V : \mathcal{X} \to \mathbb{R}_0^+$

$$V(\hat{x}) = \int_0^T \frac{1}{2}||e(s)||_Q^2 ds + \frac{1}{2}||e(T)||_{Q_f}^2 \tag{7}$$

where $e : [0, T] \to \mathbb{R}^3$ is the trajectory predicted by dynamics (2),(3) , originating at $\hat{x}$, and driven by the optimal input $u^\star(\cdot, \hat{x})$. Note also that V is positive semidefinite since it only depends on e which lies in a subset of $\mathcal{X}$ and the condition $V = 0$ characterizes the set of points on the reference path. Consider the derivative of V along the MPFC closed-loop trajectories of (2),(3), denoted as $\hat{x}(t)$,

$$\frac{dV}{dt} = \frac{\partial V}{\partial \hat{x}}\dot{\hat{x}}$$

We have that

$$\frac{\partial V}{\partial \hat{x}}\dot{\hat{x}} = \int_0^T e^T(s)Q\dot{e}(s)ds + e^T(T)Q_f\dot{e}(T).$$

Integration by parts yields

$$\frac{dV}{dt} = \frac{\partial V}{\partial \hat{x}}\dot{\hat{x}} = \frac{1}{2}e^T(s)Qe(s)\Big|_0^T + e^T(T)Q_f\dot{e}(T). \tag{8}$$

The following implication then follows directly

$$\frac{1}{2}||e(T)||_Q^2 + e^T(T)Q_f\dot{e}(T) \leq 0 \tag{9}$$

$$\Rightarrow \quad \frac{dV}{dt} \leq -\frac{1}{2}\hat{e}(t)^T Q\hat{e}(t). \tag{10}$$

Here $\hat{e}(t)$ is the closed-loop path-following error corresponding to $\hat{x}(t)$. In Theorem 7 we show that if the terminal constraints (6d), (6e) hold, then (9) is satisfied. Then, using LaSalle's invariance principle in conjunction with (10) it follows that $\hat{x}(t)$ converges to the largest invariant set such that $\dot{V} = 0 \subset \{x \in \mathcal{X} : e = 0\}$. ■

The above proof sketch relies on the quite strong assumption of recursive feasibility of OCP (6). In the next section we discuss the existence of a terminal control law enforcing (6d),(6e) ($\implies$ (9)) and recursive feasibility.

[1] Note that, for sake of simplified exposition, we consider the nominal case of recomputing the solution to (6) in an instantaneous fashion. Furthermore, we assume that, for all $\hat{x}(t)$ and $u(\cdot)$ being piecewise continuous, the OCP admits a locally optimal solution.

4. TERMINAL CONTROL AND CONSTRAINTS

4.1 Global Feasibility of (6e)*:*

For any state $q = (\vartheta, \varphi, \gamma)^T$, let

$$\mathcal{H}(q) = \{\tau^\star \,|\, \tau^\star \in \operatorname*{argmin}_\tau e(q,\tau)^T Q_f e(q,\tau)\}.$$

Also recall, $m(\tau) := \partial_\tau q_{ref}(\tau)$ and $e(q, \tau) = q - q_{ref}(\tau)$.

Lemma 2. (Minimum error points on path).
For all $\tau^\star \in \mathcal{H}(q)$, it holds that $e(q, \tau^\star)^T Q_f m(\tau^\star) = 0$. $\square$

Proof. Note that $\tau^\star \in \mathcal{H}(q)$ is a minimizer of $e^T Q_f e$. Hence, symmetry of Q_f and the first-order optimality condition imply $-e(q, \tau^\star)^T Q_f m(\tau^\star) = 0$. ■

Lemma 3. (Non-emptiness of $\mathcal{H}(q)$).
For all $q \in \mathcal{Q}$, it holds that $\mathcal{H}(q) \neq \emptyset$. $\square$

Proof. As $q_{ref}(\tau)$ is twice continuously differentiable map to a compact subset of $\mathcal{Q}$ and is periodic in τ, for any q, the term $e(q,\tau)^T Q_f e(q,\tau)$ has a minimizer. Thus optimizing over $\tau \in \mathbb{R}$ implies $\mathcal{H}(q) \neq \emptyset$. ■

Lemma 4. (Existence of neighborhoods of $\tau^\star$).
For all $\tau^\star \in \mathcal{H}(q)$, there exists a non-empty and non-singular neighborhood

$$\mathcal{N}(q, \tau^\star) := \left\{\tau \,|\, e(q,\tau)^T Q_f m(\tau) \geq 0\right\} \neq \emptyset$$

and $\mathcal{N}(q, \tau^\star) \setminus \tau^\star \neq \emptyset$.

Proof. By Lemma 2, we have $e(q, \tau^\star)^T Q_f m(\tau^\star) = 0$. Furthermore, $e(q,\tau)^T Q_f m(\tau)$ is a continuous function of τ that has a local minimum at $\tau^\star$. Hence, there exists a neighborhood of $\tau^\star$ wherein $e(q,\tau)^T Q_f m(\tau) \geq 0$. ■

Let

$$\mathcal{N}(q, \mathcal{H}(q)) := \bigcup_{\tau^\star \in \mathcal{H}(q)} \mathcal{N}(q, \tau^\star),$$

then the following theorem states feasibility of (6e).

Theorem 5. (Global feasibility of (6e)).
For any terminal condition $q(T) \in \mathcal{Q}$, there exists a $\tau(T) \in \mathbb{R}$ such that $(q(T), \tau(T))$ satisfies (6e) and is given by $\{q(T), \tau(T) : q(T) \in \mathcal{Q}, \tau(T) \in \mathcal{N}(q(T), \mathcal{H}(q(T)))\}$. $\square$

Proof. Observe that, for any given kite state $q \in \mathcal{Q}$,

$$\mathcal{N}(q, \mathcal{H}(q)) = \{\tau | e(q,\tau)^T Q_f m(\tau) \geq 0\}$$

is the set of all τ satisfying the terminal constraint (6e). Lemma 4 shows that, for all $q \in \mathcal{Q}, \mathcal{N}(q, \mathcal{H}(q)) \neq \emptyset$. Thus, independent of initial condition $q(0)$ and for any terminal state $q(T) \in \mathcal{Q}$, $\tau_T \in \mathcal{N}(q(T), \mathcal{H}(q(T)))$ satisfies (6e).

Since the considered path is periodic and we do not impose any input magnitude constraint on u_τ. Hence, for any $\tau(0)$, there exists a positive input such that $\tau(T) = \tau_T$. ■

4.2 Feasibility of (6d)*:*

For sake of readability, we drop the time argument T from vectors like $m(T), e(T), q(T)$. Recall that $\mathcal{X} := \mathcal{Q} \times \mathbb{R}$. We will also use the following short hand notations: $F(q, \tau) := (m\ e) \in \mathbb{R}^{3\times 2}$. Dropping the arguments (q, τ), we write, $g = F^T Q_f e \in \mathbb{R}^{2\times 1}$, $\quad P = F^T Q_f F$, $S = \mathrm{diag}(1, 1, 0)$ and $H = F^T S F$. Also note that we can rewrite (6d) as

$$e^T Q_f \dot{q} \leq -\frac{1}{2}||e||_Q^2.$$

Inspired by the concept of vector field controllers, let us try to find a vector field $\mathbf{v}(q,\tau) : \mathcal{X} \to \mathbb{R}^3$ such that $\dot{q}(T) = \mathbf{v}(q(T),\tau(T))$ satisfies (6e). To this end, for $\mathbf{w}(q,\tau) : \mathcal{X} \to \mathbb{R}^2$, we parametrize the desired vector field $\mathbf{v}(q,\tau)$ as

$$\mathbf{v}(q,\tau) = F(q,\tau)\mathbf{w}(q,\tau).$$

Furthermore, from (2) we have that $||\dot{q}||_S = s(q,\lambda,L,z)$ imposes a magnitude constraint on $S\dot{q}$. Thus, in order to find a $\mathbf{v}(q,\tau)$ that satisfies this magnitude constraint and satisfies (6d), we consider a optimization problem to be solved at each (q,τ) to yield a $\mathbf{w}^\star(q,\tau)$

$$\underset{\mathbf{w}\in\mathbb{R}^2}{\text{minimize}} \quad \frac{1}{2}\,||F\mathbf{w} - m||^2_{Q_f} + \frac{1}{2}||\mathbf{w}||^2 \tag{11a}$$

$$\text{subject to} \quad g^T\mathbf{w} \le -\frac{1}{2}||e||^2_Q \tag{11b}$$

$$\mathbf{w}^T H\mathbf{w} - s^2 = 0 \tag{11c}$$

where $s = s(q,\lambda,L,z)$. Note that, for the sake of readability, we dropped the arguments (q,τ) above. The penalization $||F\mathbf{w} - m||^2_{Q_f}$, in the objective function (11a), regularizes $\mathbf{w}$ such that $\mathbf{v}$ points along the tangent of the path m whenever possible. Equation (11b) imposes that $\mathbf{v}$ satisfies (6d) and (11c) imposes that $\mathbf{v}$ satisfies the magnitude constraint on $S\dot{q}$. Setting $\mathbf{w}(q,\tau) = \mathbf{w}^\star(q,\tau)$ and solving (11) yields the desired vector field $\mathbf{v}(q,\tau)$.

Proposition 8, presented in Appendix, provides the optimal solution $\mathbf{w}^\star$ to (11) and its existence conditions. Specifically, when already on the path ($e = 0$), it turns out that $\mathbf{w}^\star$ is such that $F\mathbf{w}^\star$ points along the tangent direction given by direction of m. Thus, when on the path, the desired vector field pushes the vehicle along the path, rendering the path an invariant set under the vector field. Choosing $\dot{q}(T) = \mathbf{v}(q(T),\tau(T))$, then imposes (6d).

Let $\mathcal{S} \subset \mathcal{Q}$ be a compact subset of $\mathcal{Q}$ for which the conditions of Proposition 8 are satisfied. Let $\mathcal{V}_\alpha := \{e : \frac{1}{2}||e||^2_{Q_f} \le \alpha\}$ be the largest level set contained in $\mathcal{S}$ (subject to maximization w.r.t. α). Furthermore, let $\angle\mathbf{v} = \text{atan2}(\mathbf{e}_2\mathbf{v}, \mathbf{e}_1\mathbf{v})$, $\mathbf{e}_1 = (1\ 0\ 0)$, $\mathbf{e}_2 = (0\ 1\ 0)$, $\mathbf{e}_3 = (0\ 0\ 1)$.

Assumption 5. Assume that, starting at the any $q(0) \in \mathcal{Q}$, there exists a reachable point in $\mathcal{Q}$ such that $\mathbf{v}(q(T),\tau(T)) = F(q(T),\tau(T))\mathbf{w}^*(q(T),\tau(T))$. □

Proposition 6. (Recursive feasibility of (6d)).
Let Assumption 5 hold. Then, for any $q(T) \in \mathcal{V}_\alpha$, such that $\tau(T) \in \mathcal{N}(q(T),\mathcal{H}(q(T)))$, $\gamma(T) = \angle\mathbf{v}(q(T),\tau(T))$ and $u_\gamma = \mathbf{e}_3 v(q(T),\tau(T))$, the terminal condition (6d) holds. Furthermore, the set $\mathcal{V}_\alpha$ is positively invariant and (6d) is recursively feasible. □

Proof. Observe that $\mathbf{e}_1\dot{q} = s\cos\gamma$, $\mathbf{e}_2\dot{q} = s\sin\gamma$ and $\mathbf{e}_3\dot{q} = u_\gamma$. It is easy to verify that $\gamma(T) = \angle\mathbf{v}(q(T),\tau(T))$, $u_\gamma = \mathbf{e}_3\mathbf{v}(q(T),\tau(T))$ and (11c) imply $\dot{q}(T) = \mathbf{v}$. From (11b) we have $\mathbf{v}$ such that $\dot{q}(T) = \mathbf{v}$ satisfies (6d). Furthermore, considering the positive semidefinite function $V_T(q,\tau) = \frac{1}{2}||e||^2_{Q_f}$, we see that $\dot{V}_T = e^TQ_f\dot{e} = e^TQ_f\dot{q} - e^TQ_fm(\tau)u_\tau$. Since $\tau(T) \in \mathcal{N}(q(T),\mathcal{H}(q(T)))$ is such that $e^TQ_fm(\tau) \ge 0$ and $u_\tau \ge 0$, we have $e^TQ_fm(\tau)u_\tau \ge 0$ implying $\dot{V}_T \le e^TQ_f\dot{q}$. Further with $\dot{q} = \mathbf{v}$, from (11b), we have $e^TQ_f\dot{q} \le -\frac{1}{2}||e||^2_Q$ implying $\dot{V}_T \le -\frac{1}{2}||e||^2_Q$. This implies that $\mathcal{V}_\alpha$ is positively invariant and thus (6d) is recursively feasible. ■

4.3 Convergence Constraints

Theorem 7. If (6d) and (6e) hold for a terminal state $x(T) = (q(T),\tau(T))$, then (9) also holds for $x(T)$. □

Proof. For sake readability, let us drop the time argument T with the understanding that all quantities in the expressions below are at the terminal time T. Consider

$$\frac{1}{2}||e||^2_Q + e^TQ_f\dot{e} = \frac{1}{2}||e||^2_Q + e^TQ_f\dot{q} - e^TQ_fm(\tau)u_\tau.$$

Then from (6d), it follows that $e^TQ_f\dot{q} \le -\frac{1}{2}||e||^2_Q$. Furthermore, from (6e) we have that, for all $u_\tau \ge 0$, $-e^TQ_fm(\tau)u_\tau \le 0$. These statements imply that

$$\frac{1}{2}||e||^2_Q + e^TQ_f\dot{e} \le 0.$$

This finishes the proof. ■

5. SIMULATION RESULTS

For the numerical implementation of our continuous time MPFC scheme we use a sampled data implementation with sampling time δ. The OCP (6) in the sampled data setting is solved using a direct multiple shooting approach with N time step horizon ($T = N \cdot \delta$). The nonlinear program (NLP) is setup with automatic differentiation using CasADi (Andersson (2013)) with a RK4 integrator approximation and solved using an interior point solver (IPOPT, Wächter and Biegler (2006)) on a 2.8 GHz Intel Core i7 processor. The values for Q, Q_f, R, N, T are given in (12) in the Appendix.

Subsequently, we discuss results for the following scenarios:

(1) Nominal simulations: Simulations under zero plant-model mismatch
(2) Perturbed simulations:
  (a) Sampled velocity: Speed of the vehicle is sampled at the beginning of the MPC horizon and then assumed constant at that value over the horizon.
  (b) Pumping cycle: The vehicle is reeled in and out with an external controller. The tether length is sampled at the beginning of the horizon and assumed constant over the horizon. The vehicle speed held constant as done in 2a.
(3) MPFC without terminal constraints

Note that in the perturbed scenarios 2a,2b, the AWE system is still simulated using the nominal model in equation (2), while the perturbed models as described in 2a,2b are used for predictions in the MPFC controller. Simulations without the terminal constraints are presented to highlight the role of terminal convergence constraints in enforcing faster convergence.

Nominal simulations: The first 30 seconds of Figure 2 and 3 provide a typical MPFC closed loop trajectory for the AWE vehicle under nominal simulation when following a lemniscate shaped reference path (see Appendix, (13)). Figure 3 shows the closed loop evolution of the system state $\hat{x}(t)$ and closed loop inputs $\hat{u}_\gamma(t), \hat{u}_\tau(t)$ when tracking the lemniscate. With $\delta = 0.1s$ and $N = 10$, the average solve time to plan a 1 s long horizon is 0.2 s, suggesting the possibility to apply the nominal MPFC scheme in real time

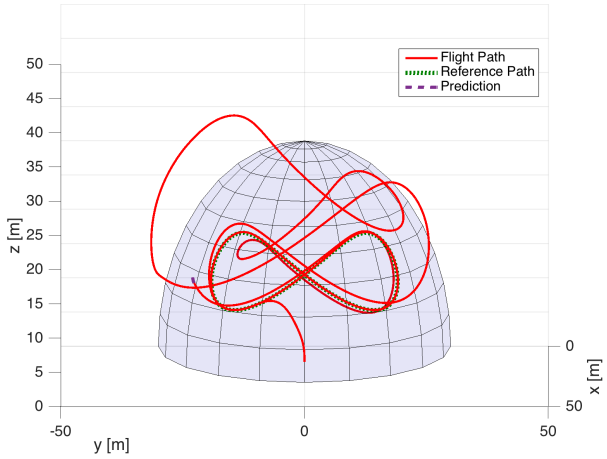

Fig. 2. Closed loop flight trajectory with convergence constraints for complete pumping cycle.

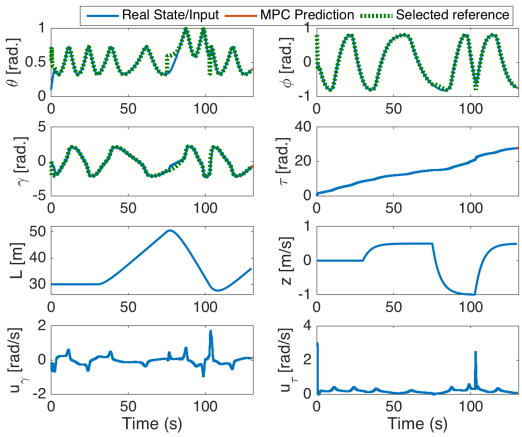

Fig. 3. Closed loop state and input evolution.

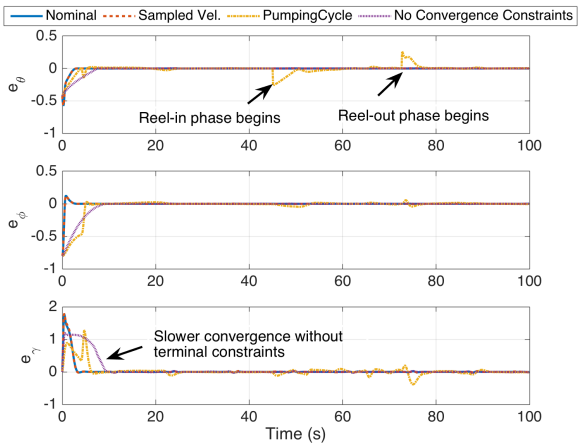

Fig. 4. Path following errors.

as a higher level planner in a cascaded structure control scheme.

Perturbed simulations: We test our control scheme applying perturbations in the velocity model $s(q, \lambda, L, z)$. Since we do not have an accurate model $s(q, \lambda, L, z)$ due to unknown parametric and structural uncertainties, we choose a simplified model where, $s(q, \lambda, L, z) = s_o$. The constant s_o is updated to the speed estimate of the vehicle at the beginning of the horizon and then held constant for the MPC prediction over the horizon. Figure 4 shows the closed loop path following error obtained under the perturbation 2a showing a very close overlap with the nominal case. Thus the MPFC scheme seems to have sufficient inherent robustness with the chosen parameters to plan under imperfect prediction. Further due to the simplification of the dynamics under this sampled speed model, the solve time is significantly reduced with an average solve time of about 0.05 seconds and worst case solve time of about 0.1 second.

The trajectory after 30 seconds in Figure 2 and 3 shows the closed loop trajectory for the complete pumping cycle operation of an AWE system corresponding to perturbation 2b. Figure 4 shows the path following errors for perturbation 2b, where the closed loop trajectory follows a reference for the full pumping cycle which is made up by switching between two different lemniscate paths for the traction and retraction phases. The switching of reference path creates an instantaneous increase in the path following error which is reduced quickly by the MPFC scheme to start tracking the new reference path.

Performance without terminal constraints: Figure 4 also shows the convergence of path following errors when terminal constraints are not imposed. This shows that the MPFC scheme can also work with only the terminal penalty being imposed. However by comparison, the terminal constraints significantly improve the convergence rates.

6. CONCLUSION

The paper presented a nonlinear model predictive path following (MPFC) scheme for airborne wind energy systems that may be used as a high-level planner in combination with a low-level steering controller. A novel set of terminal convergence field constraints are introduced to guarantee asymptotic convergence to zero path tracking error. Recursive feasibility and convergence results have been investigated for the proposed scheme under a reachability assumption for the convergence field. Numerical studies under nominal and perturbed conditions indicate good control performance. The proposed MPFC scheme is observed to be computationally viable for real-time application in cascaded kite control schemes.

APPENDIX

Simulation parameters

MPFC parameters:

$$Q = \mathrm{diag}(1000, 1000, 3), \quad Q_f = \mathrm{diag}(500, 500, 150)$$
$$R = \mathrm{diag}(0.1, 0.01), N = 10, \delta = 0.1sec., u_\gamma^{max} = 20 \tag{12}$$

Model data:

$$\mathcal{Q} = \{(\vartheta, \varphi, \gamma) : \vartheta \in [0, \pi/2), \varphi \in (-\pi/2, \pi/2), \gamma \in [-\pi, \pi]\}$$

$$s(q, \lambda, L, z) = \begin{pmatrix} 1 & 0 \\ 0 & (\cos\vartheta)^{-1} \end{pmatrix} v_w L^{-1} \begin{pmatrix} \cos\gamma \\ \sin\gamma \\ -E \end{pmatrix}^T \begin{pmatrix} -\sin\vartheta\cos\varphi \\ -\sin\varphi \\ -\cos\vartheta\cos\varphi \end{pmatrix}$$

$\Lambda = (v_w, E)$ are the parameters, wind vector and aerodynamic glide ratio respectively. ($v_w \in \mathbb{R}^2$ vector represents the wind vector in the horizontal ground plane)

Reference path parameterization: For the lemniscate reference path used in numerical simulations, we use,

$$\vartheta_{ref}(\tau) = h + a\sin(2\tau), \quad \varphi_{ref}(\tau) \quad = 4a\cos(\tau) \tag{13}$$

In perturbed scenario 2b we use $h = \pi/6$ for reel-out and $h = \pi/4$ for reel-in. $a = 0.2$ for all cases. The tether is reeled-out at 0.5 m/s and reeled-in at 1 m/s.

Terminal convergence constraints

Below adj$(\cdot)$ represents the adjoint of a matrix and trace$(\cdot)$ gives the trace of a matrix. Let, $F := (m\ e) \in \mathbb{R}^{3\times 2}$, $g := F^T Q_f e \in \mathbb{R}^{2\times 1}$, $P = F^T Q_f F$, $H = F^T S F$ and

$$\ell = -2||g||^2_{\mathrm{adj}(H)}, \quad c = -||g||^2_{\mathrm{adj}(P)} - ||g||^2$$
$$b_0 = -g^T h - g^T \operatorname{adj}(P) h - \frac{1}{2}(|P| + 1 + \operatorname{trace}(P))||e||^2_Q$$
$$b_1 = -2g^T \operatorname{adj}(H) h + (\operatorname{trace}(H) + \operatorname{trace}(H \operatorname{adj}(P)))||e||^2_Q$$
$$b_2 = 4|H|||e||^2_Q,\ r_0 = b_0 \pm cs, r_1 = b_1 \pm \ell s, \quad r_2 = b_2$$

The variable s is the speed as defined in (11).

$$\alpha_0 = -\operatorname{adj}(gg^T)h + \frac{1}{2}(I + \operatorname{adj}(P))g||e||^2_Q$$
$$\alpha_1 = -2\operatorname{adj}(H)g||e||^2_Q,\ \beta_0 = h + \operatorname{adj}(P)h$$
$$\beta_1 = 2\operatorname{adj}(H)h,\ h = \begin{pmatrix} ||m||^2_{Q_f} \\ m^T Q_f e \end{pmatrix}$$

$$k_0 = |P| + \operatorname{trace}(P) + 1,\ k_2 = 4|H|$$
$$k_1 = 2\operatorname{trace}(H) + 2\operatorname{trace}(H \operatorname{adj}(P))$$
$$n_0 = k_0 s \pm \beta_0, \quad n_1 = k_1 s \pm \beta_1, \quad n_2 = k_2 s$$

$$\lambda(\nu) = \frac{1}{\ell\nu + c}(b_2\nu^2 + b_1\nu + b_0) \tag{14a}$$
$$\text{for } \nu \in \mathcal{P}_1 := \{x \in \mathbb{R} : r_2 x^2 + r_1 x + r_0 = 0\} \tag{14b}$$

also let,

$$\mathcal{P}_0 = \{x \in \mathbb{R} : n_2 x^2 + n_1 x + n_0 = 0\} \tag{15}$$

Proposition 8. The minimizing solution for (11) is

$$\mathbf{w}^\star = \frac{1}{\sigma(\mu)}(a_1\mu + a_0) \tag{16a}$$

with $\mu \in \mathcal{P}_\lambda$ such that, for $e \neq 0, \lambda(\nu) > 0$,

$$\mathcal{P}_\lambda = \mathcal{P}_1,\ \&\ (a_1, a_0) = (\alpha_1, \alpha_0), \quad \sigma(\mu) = \ell\mu + c. \tag{16b}$$

Otherwise

$$\mathcal{P}_\lambda = \mathcal{P}_0, \quad (a_1, a_0) = (\beta_1, \beta_0), \quad \sigma(\mu) = k_2\mu^2 + k_1\mu + k_0. \tag{16c}$$

The solution exists if the quadratics defining $\mathcal{P}_0$ and $\mathcal{P}_1$ have real roots . □

Proof. The proof follows by writing the Lagrangian for (11) as

$$\mathcal{L}(w, \lambda, \mu) = \frac{1}{2}||F\mathbf{w} - m||^2_{Q_f} + \frac{1}{2}||\mathbf{w}||^2 + \lambda\left(g^T w + \frac{1}{2}||e||^2_Q\right) + \mu\left(\mathbf{w}^T H \mathbf{w} - s^2\right). \tag{17}$$

Then, writing the KKT conditions and solving for the two cases, $\lambda > 0$ and $\lambda = 0$. For $\lambda > 0$, we can write $\mathbf{w}^\star, \lambda$ as a function of μ as given in (14a) for $\mu = \nu$. μ itself can be obtained as roots to a quadratic equation (14b) with $\mu = \nu$. When $e = 0$, the inequality becomes weakly active and thus the solution can be obtained from the $\lambda = 0$ case. For $\lambda = 0$, μ can be obtained as roots to the quadratic as defined in (15). Once μ is taken for the appropriate case, $\mathbf{w}^\star$ can be obtained as specified by (16). ■

REFERENCES

Andersson, J. (2013). *A General-Purpose Software Framework for Dynamic Optimization*. PhD thesis, Arenberg Doctoral School, KU Leuven, Department of Electrical Engineering (ESAT/SCD) and Optimization in Engineering Center, Kasteelpark Arenberg 10, 3001-Heverlee, Belgium.

Diwale, S., Alessandretti, A., Lymperopoulos, I., and Jones, C.N. (2016). A nonlinear adaptive controller for airborne wind energy systems. In *American Control Conference (ACC), 2016*, 4101–4106. American Automatic Control Council (AACC).

Erhard, M., Horn, G., and Diehl, M. (2015). A quaternion-based model for optimal control of the SkySails airborne wind energy system. *arXiv:1508.05494*.

Erhard, M. and Strauch, H. (2014). Flight control of tethered kites and winch control for autonomous airborne wind energy generation in pumping cycles. *CoRR*, abs/1409.3083.

Fagiano, L., Zgraggen, A., Morari, M., and Khammash, M. (2014). Automatic crosswind flight of tethered wings for airborne wind energy: Modeling, control design, and experimental results. *Control Systems Technology, IEEE Transactions on*, 22(4), 1433–1447.

Faulwasser, T. and Findeisen, R. (2016). Nonlinear model predictive control for constrained output path following. *IEEE Trans. Automat. Contr.*, 61(4), 1026–1039.

Gros, S., Zanon, M., and Diehl, M. (2013). Control of airborne wind energy systems based on nonlinear model predictive control amp; moving horizon estimation. In *Control Conference (ECC), 2013 European*, 1017–1022.

Houska, B. and Diehl, M. (2007). Optimal control for power generating kites. In *In Proceedings of the 9th European Control Conference, Kos, Greece*, 35603567.

Houska, B. and Diehl, M. (2010). Robustness and stability optimization of power generating kite systems in a periodic pumping mode. In *Control Applications (CCA), 2010 IEEE International Conference on*, 2172–2177.

Ilzhfer, A., Houska, B., and Diehl, M. (2007). Nonlinear mpc of kites under varying wind conditions for a new class of large-scale wind power generators. *International Journal of Robust and Nonlinear Control*, 17(17), 1590–1599.

Loyd, M.L. (1980). Crosswind kite power. *Journal of Energy*, 4, 106–111.

Luchsinger, R. (2013). Pumping cycle kite power. In U. Ahrens, M. Diehl, and R. Schmehl (eds.), *Airborne Wind Energy*, Green Energy and Technology, 47–64. Springer Berlin Heidelberg.

Panagou, D., Tanner, H.G., and Kyriakopoulos, K.J. (2011). Control of nonholonomic systems using reference vector fields. In *2011 50th IEEE Conference on Decision and Control and European Control Conference*, 2831–2836. IEEE.

Topogonov, V. (2006). *Differential Geometry of Curves and Surfaces - A Concise Guide*. Birkhäuser, Boston.

Wächter, A. and Biegler, L.T. (2006). On the implementation of an interior-point filter line-search algorithm for large-scale nonlinear programming. *Mathematical Programming*, 106(1), 25–57.